Real-Time Prediction of Neurally Mediated Syncope

R. Couceiro, P. Carvalho, R. P. Paiva, J. Muehlsteff, J. Henriques, C. Eickholt, C. Brinkmeyer, M. Kelm, and C. Meyer

***Abstract*—Neurally mediated syncope (NMS) patients suffer from sudden loss of consciousness, which is associated with a high rate of falls and hospitalization. NMS negatively impacts a subject's quality of life and is a growing cost issue in our aging society, as its incidence increases with age. In this paper, we present a solution for prediction of NMS, which is based on the analysis of the electrocardiogram (ECG) and photoplethysmogram (PPG) alone. Several parameters extracted from ECG and PPG, associated with reflectory mechanisms underlying NMS in previous publications, were combined in a single algorithm to detect impending syncope. The proposed algorithm was evaluated in a population of 43 subjects. The feature selection, distance metric selection, and optimal threshold were performed in a subset of 30 patients, while the remaining data from 13 patients were used to test the final solution. Additionally, a leave-one-out cross-validation scheme was also used to evaluate the performance of the proposed algorithm yielding the following results: sensitivity (SE)—95.2%; specificity (SP)—95.4%; positive predictive value (PPV)—90.9%; false-positive rate per hour (FPRh)—0.14 h^{-1}, and prediction time (aPTime)—116.4 s.**

***Index Terms*—Autonomic nervous system, blood pressure regulation and variability, electrocardiogram (ECG), neurally mediated syncope (NMS), photoplethysmogram (PPG).**

I. Introduction

SYNCOPE is a transient and self-limiting loss of consciousness, resulting from a transient global cerebral hypoperfusion and is characterized by a rapid onset, short duration, and spontaneous complete recovery [1]. Also referred to as vasovagal and neurocardiogenic syncope, NMS belongs to a broader group of syncope known as reflex syncope, which is responsible for 21% of syncope episodes [1].

In the latest Framingham study [2] involving 7814 participants between 20 and 96 years old, it was reported an incidence rate of 6.2 per 1000 person-years. Moreover, the incidence of syncope was shown to increase with age, ranging from 2.6 to 5.4 per 1000 person-years between 20 and 69 years old. The same study shows a sharp rise to 11.1 and 19.5 per 1000 person-years within the 70–79 and above 80 years old populations [2], [3].

The main causes of syncope are generally benign. However, it is associated with frequent hospitalizations and accounts for 1–3% of all emergency department (ED) visits, as well as 1–6% of all hospital admissions in general [2], [4]. Moreover, in the U.S. approximately 4% of syncope patients discharged from the ED experience severe adverse events (e.g., readmission or death) within 72 h [4].

The recurrence of syncope episodes gains special emphasis in elderly populations, where morbidity is particularly high. Fear of falling often leads to reduced physical and social activity, which is associated with increased mental decline and incidence of medical conditions. Subsequent institutionalization is a common consequence of syncope in this age group [1].

The main advances in syncope treatment and prevention focus on lifestyle modifications, which include the education of patients regarding the awareness and avoidance of triggers, the early recognition of prodromal symptoms, and performance of counter measures to abort the syncope episode [1]. Thus, the development of a noninvasive and nonintrusive, as well as cost-efficient personal p-health system to alert patients in case of an impending syncope might: 1) provide an opportunity for the patient to perform early countermaneuvers (e.g., physical counterpressure maneuvers—PCMs) and avoid or delay syncope, as well as 2) help in diagnostics of underlying pathophysiological mechanisms with better personalized treatment options.

A. Background and State of the Art

Orthostatic intolerance is thought to be one of the most common triggers of reflex syncope [5]. Investigators believe that the abrupt and excessive amount of venous blood pooling during standing posture is responsible for a decrease in the venous blood return to the heart resulting in more vigorously ventricle contractions and excessive stimulation of the ventricular mechanoreceptors. As a result, a "paradoxical" withdrawal in sympathetic tone can occur, i.e., cardioinhibition and vasodepression. This process is associated with a decrease in blood pressure and finally syncope [6]. Although the increase in parasympathetic activity (cardioinhibition) is commonly observed during NMS, hypotension due to vasodepression is considered as the primary mechanism leading to the loss of consciousness [7].

Several studies have been proposed in the literature for NMS prediction, differing on the objectives, methods and used modalities. The most common approach is the early prediction of the head-up tilt table test (HUTT) outcome based on an analysis of HR and BP parameters before and after tilt, i.e., during the

Manuscript received August 25, 2014; revised February 11, 2015 and December 16, 2014; accepted February 25, 2015. Date of publication March 5, 2015; date of current version March 3, 2016. This work was supported by Center for Informatics and Systems of University of Coimbra and by EU projects HeartCycle (FP7-216695), iCIS (CENTRO-07-ST24-FEDER-002003), Welcome (FP7-ICT-2013-10), and HeartSafe (PTDC-EEI-PRO-2857-2012).

R. Couceiro, P. Carvalho, R. P. Paiva, and J. Henriques are with the Department of Informatics Engineering, Science and Technology Faculty, University of Coimbra, Coimbra 3000-370, Portugal (e-mail: rcouceir@dei.uc.pt; carvalho@dei.uc.pt; ruipedro@dei.uc.pt; jh@dei.uc.pt).

J. Muehlsteff is with Philips Research Laboratories Europe, Eindhoven 5600 JA, The Netherlands (e-mail: Jens.Muehlsteff@philips.com).

C. Eickholt, C. Brinkmeyer, M. Kelm, and C. Meyer are with the Division of Cardiology, Pneumology, and Angiology, Heinrich-Heine University Hospital Düsseldorf, Düsseldorf 40225, Germany and also with the Department of Electrophysiology, University Heart Center, University Hospital Eppendorf, Hamburg 20246, Germany (e-mail: Christian.Eickholt@med.uni-duesseldorf.de; Christoph.Brinkmeyer@med.uni-duesseldorf.de; Malte.Kelm@med.uni-duesseldorf.de; Christian.Meyer@med.uni-duesseldorf.de).

Color versions of one or more of the figures in this paper are available online at http://ieeexplore.ieee.org.

Digital Object Identifier 10.1109/JBHI.2015.2408994

2168-2194 © 2015 IEEE. Personal use is permitted, but republication/redistribution requires IEEE permission.
See http://www.ieee.org/publications_standards/publications/rights/index.html for more information.

supine position and early passive standing position. These methods are mainly focused on the analysis of the HR and/or SBP variability using either time- or frequency-domain techniques, or both. The time-domain methods focus on the evaluation of temporal changes of HR during the supine and upright positions, using statistical features, such as mean, standard deviation [8]–[11], variance and kurtosis [12], or even doing simple comparisons between the HR in both phases [13], [14]. The frequency-domain methods are mainly based on the evaluation of the characteristics of the low (LFr: 0.04–0.15 Hz) and high (HFr: 0.15–0.40 Hz) frequency components (e.g., power and area) and on the relationship between the characteristics of those components (the LFr/HFr ratio) as measures of sympathovagal balance [10], [11], [15]–[17]. Additionally, methods using indices of myocardial contractility assessed from peak endocardial acceleration [18], from transthoracic impedance cardiography (ICG) [19], [20] and from the arterial blood pressure waveform [21] have also been proposed in the literature.

In contrast with the early prediction approach, the real-time prediction problem has only been addressed in the later years, where hemodynamic changes are continuously monitored during the whole HUTT protocol. Rather than focusing on the hemodynamic responses resulting from the change of posture, the real-time approaches continuously assess the risk of an impending syncope episode from the monitored hemodynamic parameters. Since the mechanisms underlying the occurrence of syncope are characterized by fast dynamics and are not limited to changes of posture, these approaches are believed to have a wider scope concerning the real-life scenarios. Here, the changes in heart rate (HR) and continuously measured systolic blood pressure (SBP) have also been considered [22], [23]. Virag *et al*. [22] proposed a method for real-time prediction of impending syncope based on the time and frequency analysis of the HR and SBP signals, while Mereu *et al.* [23] evaluated the prediction ability of HR and BP (SBP, MBP, DBP, and PP) trends and the ratio between the dRR (first derivative of RR) with those trends. However, current noninvasive blood pressure monitoring systems have several disadvantages. Most obviously their application is cumbersome due to bulky and expensive hardware, as well as complicated handling with the need for frequent calibrations [24]. These limitations become critical in unsupervised environments such as at home or in ambulatory scenarios, where low cost and easy-to-use devices are essential. More recently, several authors focused on the evaluation of changes of the pulse arrival time (PAT) alone [25], as a surrogate for SBP changes, or combined with HR changes [26], [27] and, finally, prediction of syncope. In our previous works [25], [28], we established and validated a method for syncope prediction using PAT and evaluated the possible mechanisms underlying the development of NMS.

B. Main Contributions and Paper Organization

In this paper, we propose a complete framework with tailored algorithms for prediction of NMS by analyzing changes of several cardiovascular parameters that characterize the chronotropic (HR), inotropic (left ventricular ejection time—LVET), vascular tone and blood pressure (PAT, stiffness index—SI, and reflection index—RI). These parameters were extracted from the joint analysis of the electrocardiogram (ECG) and photoplethysmogram (PPG), which can be acquired easily and nonobtrusively with state-of-the-art equipment. The parameters were normalized and led to the definition of ten features. The best seven features were selected and the distance to the orthostatic reference was calculated using the Minkowski distance metric. A threshold-based approach was adopted to detect impending syncope.

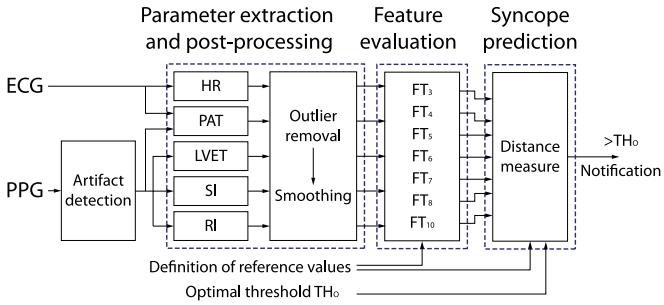

Fig. 1. Schematic representation of the proposed algorithm structure. HR, PAT, left ventricular ejection (LVET), SI and RI are extracted from the analysis ECG and PPG, which are postprocessed and evaluated in order to extract seven features. Syncope prediction is performed using a threshold-based approach applied to the distance of the extracted features to an orthostatic stable reference. A notification is generated if the distance measure surpasses a predefined optimal threshold (TH_O).

The remainder of this paper is organized as follows. The proposed solution for syncope prediction is presented in Section II. The experimental protocol used in the present study is described in Section III. The main results and respective discussion are presented in Section IV. Finally, we present our main conclusions in Section V.

II. Methods

The main steps of the proposed solution are illustrated in Fig. 1, which are: 1) detection of motion artifacts; 2) parameter extraction and postprocessing; 3) feature evaluation; and 4) syncope prediction.

A. Detection of Motion Artifacts

It is well known that the PPG signal is prone to several sources of error (e.g., motion artifacts), which can be a serious obstacle in the reliable extraction of the derived parameters, especially in uncontrolled environments such as home care and ambulatory scenarios. Therefore, it is important to detect the sections of the PPG signal that are corrupted and consequently shall not be included in the subsequent steps of the analysis. In the proposed framework, we adopted a motion artifact detection algorithm using features from the time and period domain of the PPG signal [29]. The classification of the corrupted/clean PPG sections is performed using a C-support vector classification (C-SVC) algorithm [30], with a radial basis function kernel. The classification model was fed with eight inputs calculated from the rate of change of the time- and period-domain characteristics of the

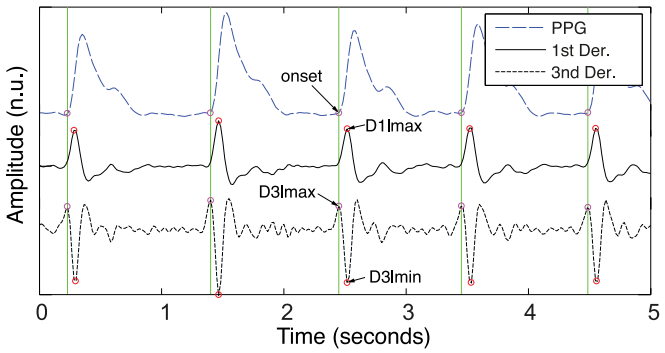

Fig. 2. Segmentation of the PPG using a multiple-order derivative analysis approach.

PPG signal. The time-domain features were extracted from the morphological characteristics of the PPG signal:

1) *Pulse amplitude*—difference between the pulse peak height and its preceding trough depth (pulse onset);
2) *Trough depth difference*—difference between the foot height of consecutive pulses;
3) *Pulse skewness*—evaluation of the pulse symmetry;
4) *Pulse kurtosis*—evaluation of the pulse "peakedness"

To extract the period-domain features, the discrete-time short-time Fourier transform was applied, and the most relevant characteristics of the spectra were evaluated: 1) location of the spectrum second major spike; 2) location of the spectrum third major spike; 3) length of the spectrum third major spike; and 4) ratio between the area of the three major spikes and the area of the remaining spectrum.

B. Parameter Extraction

Chronotropic and inotropic changes were assessed via HR and LVET.

The HR was derived from the analysis of the ECG signal and was defined as the time span between consecutive R-peaks, detected by a Pan–Tompkins algorithm [31].

The LVET was assessed from the PPG analysis using an extension of the algorithm proposed in [32]. First, the PPG signal is band-pass filtered in a 0.23–18 Hz frequency band to remove high frequency noise and the baseline fluctuations. Second, the onset of each PPG pulse is detected using a multiple-order derivative analysis approach. Derivatives from order 1–3 (f'_{ppg} to f'''_{ppg}, respectively) are calculated using a five-point digital differentiator [22] and the onset of each PPG pulse is defined as the local maxima (D3lmax) on the f'''_{ppg} preceding the local minima (D3lmin) that corresponds to the f'_{ppg} local maxima (D1lmax), as presented in Fig. 2. To detect the D1lmax, a cumulative histogram of the f'_{ppg} data is calculated and the threshold $\mathrm{ThR_{PPG}}$ is defined as the greater value bellow which 90% of the observations are found. The f'_{ppg} local maxima with absolute amplitudes greater than $\mathrm{ThR_{PPG}}$ are defined as D1lmax [33].

Each extracted PPG pulse was normalized to the unit, the linear trend was removed and the systolic and diastolic phases were identified. The systolic phase associated with the ventricular ejection was defined between the onset of the PPG pulse and the onset of the dicrotic notch (or inflection). The diastolic phase, resulting from pulse reflections in the arterial path, was defined as the portion of the PPG pulse between the offset of the dicrotic notch and the offset of the PPG pulse, as presented in Fig. 3 (top). The onset/offset of the dicrotic notch was defined as the negative-to-positive/positive-to-negative zero crossings between 0.2 and 0.4 s [34].

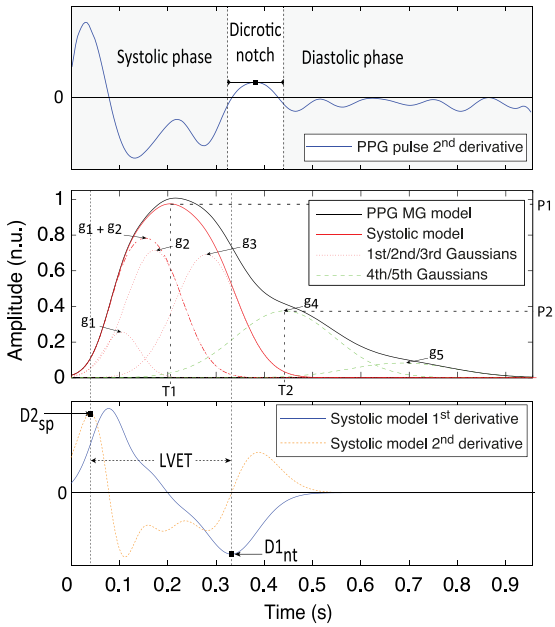

Fig. 3. Schematic representation of the approach used to determine LVET, SI, and RI. Top: Second derivative of the PPG pulse for determination of the systolic and diastolic phases. Middle: Gaussian model of the PPG pulse and the characteristic points used to assess SI and RI, respectively. Bottom: First and second derivatives of the systolic model used to determine LVET.

The systolic and diastolic phases were modeled by a sum of three and two Gaussian function, respectively, and PPG pulse model was defined as follows:

$$f_m\left(t,\beta_j\right)=\sum_{j=1}^{5}a_j e^{\frac{-\left(t-c_j\right)^2}{2b_j^2}},\quad \beta_j=\{a,b,c\}_j \tag{1}$$

where the parameters a_j, b_j, and c_j correspond to the amplitude, location, and length of the Gaussian function j. The sum of the first and second Gaussians (g_1+g_2) corresponds to the wave driven by the systolic ejection. The third Gaussian (g_3) is related to the first pulse reflection at the junction between the thoracic and abdominal aorta, presented in Fig. 3 (middle). The fourth and fifth Gaussians (g_4 and g_5) derive from forward pulse reflection at the juncture between abdominal aorta and common iliac arteries [35] and minor reflections and re-reflections in the systemic structure, respectively. The adjustment of the model parameters was achieved minimizing the sum of the squared residuals, using the least squares minimization method, as follows:

$$f_{\mathrm{MSE}}(\beta)=\frac{1}{N}\sum_{n=1}^{N}\left[f\left(n\right)-f_m\left(n,\beta\right)\right]^2 \tag{2}$$

where $f_m\,(n,\beta)$ is the MG model with the set of parameters $\beta_j = \{a,b,c\}_j\,, j = 1,\ldots,5$. Using the interior point algorithm [36], the goal is to solve nonlinear constrained optimization problem presented in

$$\begin{array}{ll} \min & f_{\mathrm{MSE}}(\beta) \\ \text{subject to} & g\,(\beta) \leq 0 \\ & lb \leq \beta \leq ub \end{array} \tag{3}$$

where $g\,(\beta) \leq 0$ and $lb \leq \beta \leq ub$ are the physiologically driven inequality constrains and the boundaries to which the parameters are subject.

The LVET was defined by the time span between systolic peak of the systolic model second derivative ($D2_{sp}$) and the notch in the systolic model first derivative ($D1_{nt}$), as presented in Fig. 3 (bottom).

To assess vascular and blood pressure changes, three highly pressure dependent parameters were also extracted [25], [35], [37], [38]. The SI is associated with the velocity of a pulse wave in large arteries [39] and correlates with pulse pressure [35] was defined as the time span between the forward wave ($g_1 + g_2 + g_3$) and the reflected wave (g_4) and is described by:

$$\mathrm{SI} = T2 - T1 \tag{4}$$

where the *T*1 is the time index corresponding to the maximum of the forward wave ($g_1 + g_2 + g_3$) and the *T*2 is the time index corresponding to the peak of the reflected wave (g_4), as indicated in Fig. 3 (middle).

The RI, associated with small artery stiffness [39], was defined as the ratio between the amplitudes of the forward wave ($g_1 + g_2 + g_3$) and the reflected wave (g_4) and is described by:

$$\mathrm{RI} = P2/P1 \tag{5}$$

where *P*1 is the amplitude of the forward wave ($g_1 + g_2 + g_3$) and *P*2 is the amplitude of the reflected wave (g_4), as indicated in Fig. 3 (middle).

Finally, $\mathrm{PAT}_{80\%}$ was defined as the time span between the ECG R-peak and the moment in time corresponding to 80% of the PPG pulse amplitude after its onset, which is known to correlate well with a decreasing BP in NMS [11].

C. Parameter Postprocessing

The presence of motion artifacts in the ECG signal and the inappropriate behavior of the parameter extraction algorithms can lead to the appearance of spurious values that do not reflect the undergoing physiological processes and consequently in inaccurate interpretation of data. This issue can be particularly observed in unsupervised monitoring with ill-defined measurement conditions. Therefore, a postprocessing step is needed to detect and remove these spurious values. In the current framework, a sliding window boxplot analysis [40] was adopted to remove outliers from the extracted parameters. First, a smoothed version (PRs_i) of each parameter PR_i was calculated using a moving median average filter (121 beats length—presented in Fig. 4 for the LVET parameter as a red thick line). The extracted PRs_i was subtracted to the parameter time series PR_i according to

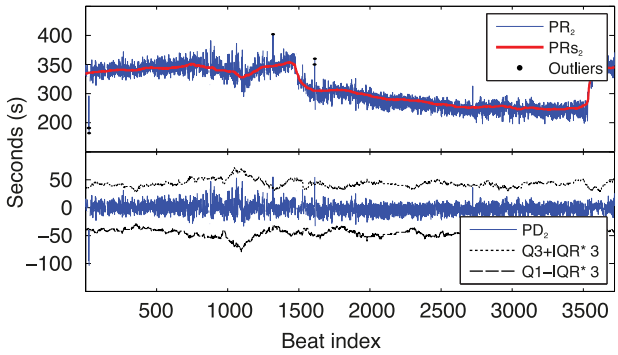

Fig. 4. Example of the adopted outlier detection approach based on a 121 beat sliding window box plot analysis. Top: Extracted LVET parameter (PR_2) smoothed LVET (PRs_2) and detected outliers. Bottom: LVET parameter difference (PD_2), and outlier detection criterion limits ($Q1 - 3^*IQR$ and $Q3 + 3^*IQR$).

$$PD_i(t) = PRs_i(t) - PR_i(t) \tag{6}$$

where $PD_i(t)$ is the resulting time series without the main trend (presented in Fig. 4 for the LVET parameter—bottom), herein called as parameter difference.

Let $PD_i^w(t) = \{PD_i(t-w,\ldots,t+w\}$ be a temporal sliding window over the derived time series PD_i with length w^*2+1 and centered in the instant *t*, for the *i*th parameter. For each window, the lower quartile (Q1: 25th percentile), the upper quartile (Q3: 75th percentile), and the interquartile range ($IQR = Q3 - Q1$) are identified. The PR_i sample at the instant *t* is considered an outlier if the corresponding PD_i sample (see Fig. 4—bottom) satisfies the following criterion:

$$PD_i\,(t) < Q1 - 3 * IQR \vee PD_i\,(t) > Q3 + 3 * IQR. \tag{7}$$

Finally, all the identified outliers are excluded from the extracted parameters time series PR_i.

The rationale behind this approach is that the sporadic parameter values resulting from artifacts and noise can be detected as outliers, which greatly differ from the parameter main trend.

Finally, the parameter time series were linearly interpolated at a 2 Hz frequency, which according to [25] is well above the required minimal sample frequency and a Butterworth low-pass filter with a 0.05 Hz cutoff frequency was used to reduce high frequency noise.

D. Feature Evaluation and Selection

To develop a robust prediction algorithm, independent from the patient's specific characteristics, the extracted parameters were normalized according to (8) and (9), resulting in a set of ten features in total (summarized in Table I). The first five features were defined as follows:

$$\mathrm{FT}_i\,(t) = \widetilde{PR}_i(t) = \frac{PR_i(t)}{PR\mathrm{ref}_i}, i = 1,\ldots,5 \tag{8}$$

where FT_i is the *i*th feature, PR_i is the *i*th parameter, $PR\mathrm{ref}_i$ is the average of each parameter during the second minute (reference window) after the patient was tilted to the upright position, and *t* is the time instant. The selection of the second minute

TABLE I
CORRESPONDENCE BETWEEN PARAMETERS/FEATURES INDEXES AND NAMES

Parameter name	Parameter index	Feature name (first set)	Feature name (second set)
HR	PR_1	$\widetilde{PR}_1$	ΔPR_1
LVET	PR_2	$\widetilde{PR}_2$	ΔPR_2
SI	PR_3	$\widetilde{PR}_3$	ΔPR_3
RI	PR_4	$\widetilde{PR}_4$	ΔPR_4
PAT	PR_5	$\widetilde{PR}_5$	ΔPR_5

as the reference window ensures that the patient achieves orthostatic stabilization, which typically occurs within less than 1 min [6].

Additionally, the normalized changes of the extracted parameters during the last 1.5 min (the minimum response time according to [25]) were also taken into account as follows:

$$\mathrm{FT}_{i+5}(t) = \Delta PR_i(t) = \frac{PR_i(t) - PR_i(t - 1.5\,\mathrm{min})}{PR\mathrm{ref}_i}, \quad i = 1, \ldots, 5. \tag{9}$$

The selection of the most appropriate features for syncope prediction was performed using the approach proposed in [41], where the features are selected based on a score metric (FSS) combining their relevance and redundancy, presented in (10). The relevance of each feature was assessed by the area under the curve (AUC) of the receiver operating characteristic (ROC) curve, while its redundancy was assessed by Spearman's rank correlation coefficient (RCC)

$$\mathrm{FSS}_i = \mathrm{AUC}(\mathrm{FT}_i) - \frac{\left|\sum_{\mathrm{FT}_j \in S} \mathrm{RCC}(\mathrm{FT}_i, \mathrm{FT}_j)\right|}{|S|} \tag{10}$$

where $\mathrm{AUC}(\mathrm{FT}_i)$ is the AUC obtained by the *i*th feature, $\mathrm{RCC}(\mathrm{FT}_i, \mathrm{FT}_j)$ is Spearman's RCC between the *i*th and *j*th feature, S is the subset of selected features at each iteration, and $|S|$ its cardinality. In sum, seven features were selected corresponding to the highest features selection scores.

1) Syncope Onset Detection Algorithm: From the analysis of the extracted features immediately before the onset of syncope, we observed significant changes in the majority of the tilt positive patients (see Fig. 5). The chronotropic and inotropic variations were reflected in a substantial decrease of ΔPR_1 and increase in ΔPR_2. Moreover, a significant drop in blood pressure was reflected in a substantial increase of $\widetilde{PR}_3$, $\widetilde{PR}_5$, ΔPR_3, ΔPR_5 and decrease of $\widetilde{PR}_4$.

To illustrate how the features vary during a HUTT, principal component analysis was applied to the selected features in two patients (with/without NMS), and a representation of the first three principal components is shown in Fig. 6. In general, for HUTT positive (po) patient, the trajectory evolves away from the orthostatic stable reference point, just before the onset of syncope. An example of this behavior is presented in Fig. 6 (top) for a 69-year-old patient with manifested syncope and GTN provocation. Contrarily, on HUTT negative (ne) patients the trajectory remains closer to the orthostatic stable state as

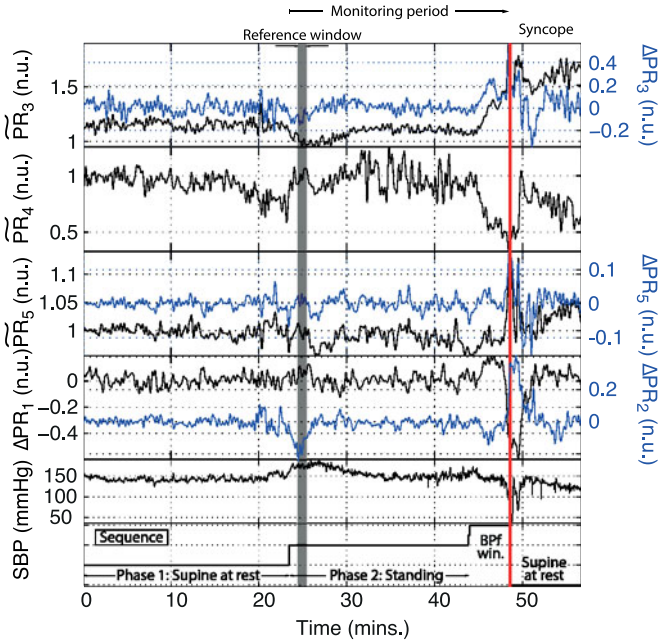

Fig. 5. HUTT of a 50-year-old patient with syncope onset during GTN provocation. Representation of the seven most discriminant features assessed from the extracted parameters, SBP and HUTT sequence.

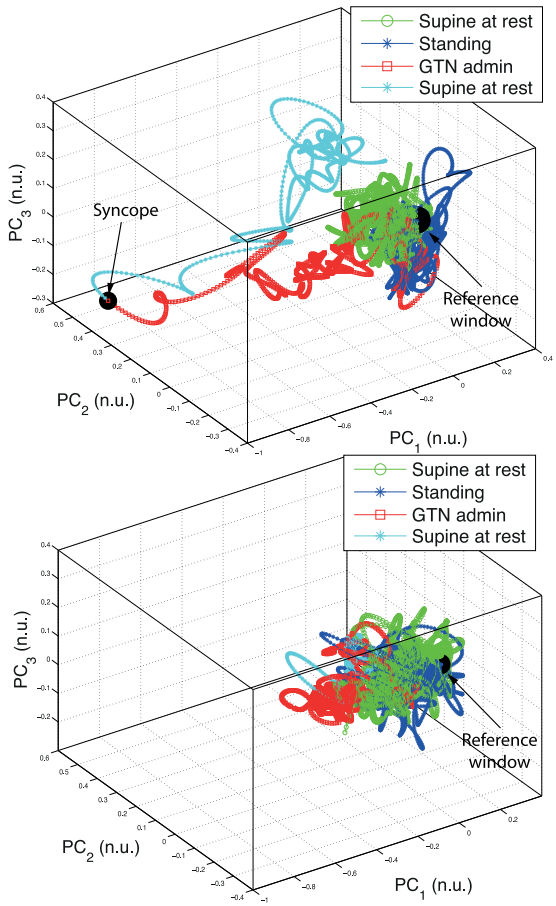

Fig. 6. Illustration of the trajectory of the three principal components extracted from the most discriminative features, during HUTT procedure. Top: 69-year-old patient with manifested syncope and GTN provocation. Bottom: 78-year-old patient with no syncope and GTN provocation.

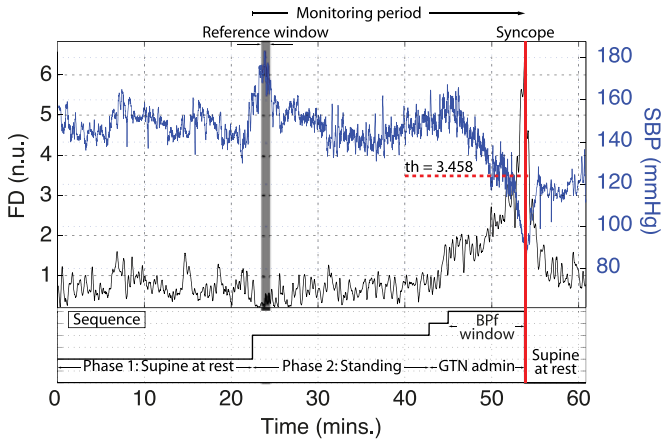

Fig. 7. HUTT of a 69-year-old patient with manifested syncope and GTN provocation. Top diagram: SBP (blue) and FD (black) time series during HUTT. Bottom diagram: Phases of HUTT. Reference window represent as a black bar, corresponding to the second minute of phase 2. BPf window corresponds time between the start of BP fall and the syncope episode.

shown in Fig. 6 (bottom) for a 78-year-old patient with no syncope after GTN administration.

These findings suggest that distance metrics might be used to differentiate the stable state from the risk of an impending event, i.e., to capture changes relative to a stable orthostatic reference at the beginning of the standing period (FTref). In order to choose the distance metric that better suits syncope prediction, several metrics were evaluated using ROC analysis combined with a fivefold cross-validation scheme. The highest F-measure was adopted as the selection criterion leading to the selection of the Minkowski distance metric ($p = 2^{-0.5}$), which was calculated according to (11). Since the proposed measure does not account for the direction of the evolving trajectory, it is necessary to eliminate feature variations that are not associated with the physiological mechanisms underlying NMS, and might negatively affect FD measure. Therefore, the ΔPR_3 and ΔPR_5 values above unit and $\widetilde{PR}_4$ values below unit were set to one. Additionally, ΔPR_1 values below zero, and ΔPR_2, ΔPR_3 and ΔPR_5 values above zero were set to zero

$$\mathrm{FD}\,(t) = \left(\sum_{i=1}^{7} \left| \mathrm{FT}_i\,(t) - \mathrm{FTref}_i \right|^p \right)^{1/p}, p = 2^{-0.5} \qquad (11)$$

where $\mathrm{FD}\,(t)$ is the Minkowski distance at the time instant *t*.

Impending NMS was detected when FD crosses a predefined optimal threshold. The SBP, FD, and HUTT sequence are presented in Fig. 7 for an example case of 69-year-old patient.

III. Data Collection

A. Study Design and HUTT Protocol

Data were acquired during scheduled diagnostic HUTT from 55 patients with unexplained syncope. All patients gave written informed consent to participate in this study (ClinicalTrials.gov identifier: NCT01262508).

TABLE II
PATIENT CHARACTERISTICS (AVG ± STD)

	Tilt positive ($n = 21$)	Tilt negative ($n = 22$)
Age [y]	57 ± 18	63 ± 17
Weight [kg]	86 ± 15	74 ± 13
BMI [kg/m^2]	27.1 ± 4.6	26 ± 5
Male/female	13/8	10/12
GTN yes/no	15/6	15/7

The HUTT protocol followed the recommendation of the European Society of Cardiology (ESC) and consisted of four phases: 1) the patient was lying at rest of at least 15 min; 2) the patient did a passive standing exercise of 20 min at a position of 70°; 3) phase (2) was extended by 15 min, if no syncope occurred, with sublingual administration of 400 μg of glycerol trinitrate (GTN); and 4) the patient was tilted back to supine position. The HUTT stopped at any moment in time, if syncope occurred and the patient was brought back to supine position immediately for recovery. The nurse accompanying the study documented any prodromal symptoms such as dizziness, sweat, tremor, etc., during the procedure.

According to the guideline of ESC, the test outcome was classified as positive (po) or negative (ne) [2]. A positive result is characterized by occurrence of syncope or presyncope with the presence of bradycardia, hypotension, or both.

Data of 12 patients had to be removed due to BP regulation failures not caused by syncope, presence of arrhythmias or poor data quality in BP and PPG signals. The characteristics of the reaming study population consisting of 43 patients are summarized in Table II.

B. Experimental Setup

The patients were monitored using two independent acquisition systems during the whole HUTT protocol.

The ECG-II lead and PPG signal (with sampling frequencies of 500 and 126 Hz, respectively) were acquired using a Philips MP50 patient monitor [42] extended with a data logger functionality. To collect the PPG signal, a standard SpO2 sensor was attached to the index finger.

Continuous noninvasive blood pressure (@50 Hz) was collected using a "Taskforce Monitor" [43]. Additionally, two ECG leads (@1000 Hz) and an ICG signal (@50 Hz) were also acquired. Based on these signals, several hemodynamic parameters are provided, such as continuous (beat-to-beat) SBP, total peripheral resistance index, and stroke volume.

The synchronization of the data coming from both systems was performed by temporally aligning the RR intervals time series extracted from ECG signals of both acquisition systems.

IV. Results and Discussion

To evaluate the performance of the proposed algorithm, two validation schemes have been adopted: 1) three-way data

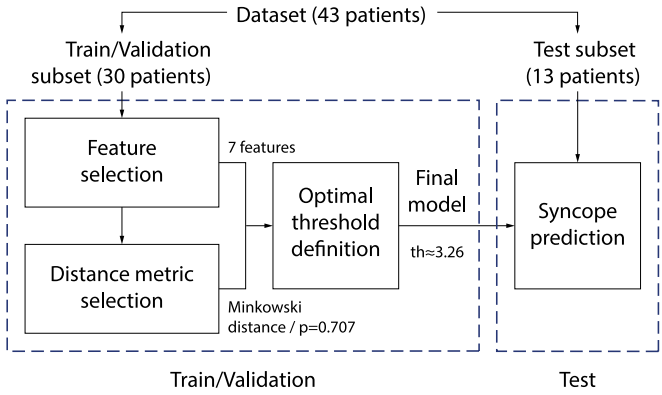

Fig. 8. Diagram of the adopted three-way data split validation scheme. Train/validation: Feature selection, distance metric selection and optimal threshold definition. Test: Evaluation of the proposed algorithm prediction capability.

split validation (shown in Fig. 8); and 2) leave-one-out cross-validation LOO CV.

In the three-way data split validation scheme, the dataset was randomly partitioned into a train/validation and test subsets. The train/validation subset was constructed in order to have approximately 70% of the study population, corresponding to 15 po patients and 15 ne patients. The remaining 13 patients (ap. 30%), i.e., six po patients and seven ne patients, were included in the test subset.

The train/validation subset was used to select the best features, evaluate the performance of the proposed algorithm, and select the optimal threshold for syncope prediction. The algorithm performance and optimal threshold were evaluated using a fivefold cross validation (5f-CV) approach (repeated 20 times). In this process, the training set (four subsets) is used to find the optimal threshold based on ROC analysis, while remaining subset is used for validation. This process was repeated for each of the five subsets (folds). The test subset was used to validate the final solution, and test the real algorithms' performance.

In the leave-one-out cross validation scheme, the dataset was partitioned into 43 subsets, corresponding to each patient. From the 43 subsets, 42 subsets were used for training and the remaining subset was used for testing. The cross-validation process was repeated 43 times with each of the 43 subsets being used exactly once as the validation data.

The proposed methodology was evaluated using the following metrics: F-measure (F-m), sensitivity (SE) and specificity (SP), positive predictive value (PPV), false-positive rate per hour (FPRh), prediction time average (aPTime), and standard deviation (sPTime).

The detection result was considered a true positive (TP) if an alarm is generated within the time window corresponding to the time between the start of BP fall and the syncope episode (BPf window). Otherwise, the detection result was considered a false positive (FP). A true negative (TN) was assigned if no alarm is generated outside the BPf window, whereas a false negative (FN) is considered if alarms are generated in this period. The FPRh was defined as the number of false-positives divided by the sum of all non-BPf windows (in hours) of all patients, while the PTime was defined as the time span between the first alarm and the syncope episode.

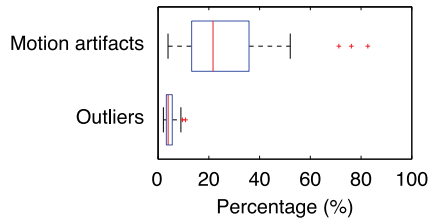

Fig. 9. Box plot of the percentage of pulses classified as motion artifacts (top) and parameter samples detected as outliers (bottom).

In the fivefold CV, the performance of the algorithm was assessed in each iteration and the average was computed. After repeating this process 20 times, the average and standard deviation ($\mathrm{avg} \pm \mathrm{std}$) of the aforementioned metrics were evaluated. In the LOO CV, the performance of the algorithm was computed based on the countings of each iteration detection result, at the end of the CV process.

A. Motion Artifacts Detection and Parameter Postprocessing

The percentage of the detected motion artifacts and outliers was assessed for each patient and the results were evaluated using a box plot analysis, which is presented in Fig. 9. It is possible to observe that the percentage of detected motion artifacts is far greater (Median: 21.64%; Mean: 26.68%) than the percentage of detected outliers (Median: 3.94%; Mean: 4.56%). Moreover, the percentage of motion artifacts detected in 3 of the 43 patients was greater than 70%. These results suggest that even in a controlled environment such as the HUTT, the PPG signal is prone to be corrupted with motion artifacts. The results also show a discrepancy between the percentage of detected motion artifacts and outliers, which can be explained by the percentage of false detections of the motion artifacts detection algorithm (approximately 10%). Another possible reason relies on the outlier detection algorithm itself. Since it is based on a boxplot analysis, it is expectable that sections corrupted with motion artifacts result in a high variance in the extracted parameters, which prevents the correct identification of outliers. These results emphasize the importance of combining both motion artifacts and outliers detection algorithms in order to increase the robustness of the syncope prediction method.

Regarding the segmentation of the PPG signal, the adopted algorithm was able to identify the PPG pulses with a sensitivity of 96.27% and a positive predictive value of 97.23% in the current dataset.

B. Feature Selection

The feature selection results are presented in Table III. One observes that the feature presenting the highest FSS refers to PAT parameter ($\widetilde{PR}_5$), followed by $\widetilde{PR}_3$, related to SI. The remaining selected features correspond to the normalized changes of HR (ΔPR_1) over a 1.5 min window and to the change of RI relatively to the reference window ($\widetilde{PR}_4$). It is also evident

TABLE III
PERFORMANCE OF THE EXTRACTED FEATURES ($FT_{1,\ldots,10}$)

Feature acronym	Score (%)	SE (%)	SP (%)	PPV (%)	FPRh (h^{-1})	aPTime (s)	sPTime (s)
$\widetilde{PR}_5$	94.6	100.0	90.0	83.3	1.7	101.0	85.4
$\widetilde{PR}_3$	89.6	80.0	96.7	92.3	0.8	125.2	121.3
ΔPR_1	75.8	80.0	86.7	75.0	2.4	60.8	72.3
$\widetilde{PR}_4$	71.0	86.7	83.3	72.2	2.0	113.2	94.2
ΔPR_5	70.7	80.0	93.3	85.7	0.8	76.4	143.0
ΔPR_3	68.3	80.0	93.3	85.7	0.3	84.5	84.3
ΔPR_2	67.4	80.0	73.3	60.0	4.1	90.2	80.6
$\widetilde{PR}_2$	56.0	93.3	60.0	53.8	5.2	201.6	130.2
$\widetilde{PR}_1$	49.0	73.3	90.0	78.6	1.2	77.0	142.7
ΔPR_4	35.9	100.0	10.0	35.7	11.3	206.7	141.8

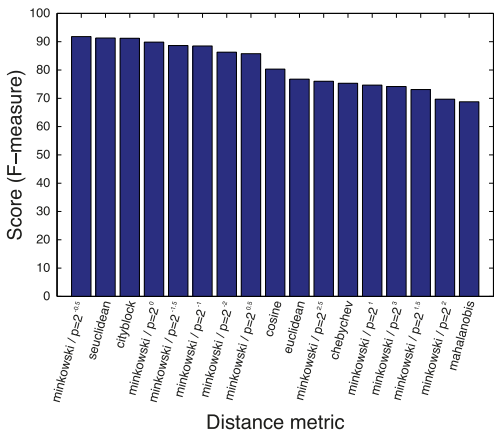

Fig. 10. Bar plot representing the scores of the evaluated distance metrics.

that between the seventh and eighth features (separated by a thick red line in Table III) there is a huge gap in the FSS score (≈11.4%). The low performance of the last three features, as indicated by the FSS decrease, resulted in the exclusion these features. In summary, seven features were selected from a total of ten extracted features. Although the best feature ($\widetilde{PR}_5$) extracted from the analysis of the PAT parameter present the highest FSS, it is worth noting that it presents lower SP (90%) and PPV (83.3%), when compared to $\widetilde{PR}_3$ (SP: 96.7% and PPV: 92.3%). Additionally, this feature presents a high FPRh (1.7 h^{-1}) when compared to the selected features, and particularly $\widetilde{PR}_3$ (0.8 h^{-1}).

The selected features with the highest prediction time (aPTime) also derive from the analysis of SI ($\widetilde{PR}_3$: 125.2 s), followed by $\widetilde{PR}_4$ (113.2 s) and $\widetilde{PR}_5$ (101.0). The aPTime of the remaining features ranges from 60.8 s (ΔPR_1) to 90.2 s (ΔPR_2).

C. Distance Metric Selection

The selection of the most appropriate distance metric was achieved using a fivefold cross-validation scheme (repeated 20 times) and the distance metric obtaining the best F-measure score was chosen. The scores obtained by each distance metric and corresponding parameters are presented in Fig. 10. As shown in Fig. 10, the distance metric presenting the best score is the Minkowski distance with parameter $p = 2^{-0.5}$ and therefore it used in the assessment of the distance between the evolving trajectory and the stable orthostatic reference.

D. Syncope Detection

The performance of the proposed algorithm was evaluated in two separate phases. First, the algorithm performance (presented in Table IV—*3W-DS validation*) and the optimal threshold were evaluated using a 5f-CV scheme (repeated 20 times) in train/validation phase. Second, the real prediction capability of the proposed solution (presented in Table IV—*3W-DS test*) was tested on the test subset using the optimal threshold (TH_0).

The optimal threshold (TH_0) was evaluated based on the following criterion:

$$\mathrm{TH}_0 = 1/N \sum_{n=1}^{N} \left(1/K \sum_{k=1}^{K} \mathrm{TH}(n,k) \right) \tag{12}$$

where TH is the threshold calculated at the iteration *k* on the 5f-CV *n*th repetition, $N = 20$ is the number of repetitions of the 5f-CV, $K = 5$ is the number of 5-f CV iterations/folds. Using (12), the optimal threshold was defined as $\mathrm{TH}_0 = 3.458$.

Additionally, the proposed algorithm performance was also evaluated using a leave-one-out cross-validation approach using the whole dataset composed of 43 patients, herein called LOO validation phase (presented in Table IV—LOO validation).

1) Influence of Motion Artifacts and Outliers: In order to evaluate the influence of the artifacts detection and outlier removal steps on the overall performance of the proposed algorithm, each of the before mentioned train/validation and test phases were performed using four sets of features, which are as follows.

1) Raw data—features extracted without removing the motion artifacts and outliers.
2) Data w/o outliers—features extracted after removing the outliers.
3) Data w/o artifacts—features extracted after removing the motion artifacts.
4) Data w/o artifacts and outliers—features extracted after removing the motion artifacts and outliers.

From Table IV, it is possible to observe that in each phase, the performance of the proposed method strongly benefits from the removal of artifacts, outliers and both. It is shown an F-measure increase, during the 3W-DS validation, of 13% with the removal of outliers, approximately 8% with the removal of artifacts and approximately 15% with the removal of both. In the 3W-DS test phase and LOO validation, similar results have been achieved with the exception to the increase in performance from the data w/o outliers to the data w/o artifacts and outliers, where no performance increase has been observed (F-measure: 3W-DS Test—92.3%; LOO *validation*—93%).

The removal of outliers and artifacts has also a significant impact on the reduction of false alarms, which can be confirmed by the decrease of the FPRh in each of the validation phases. The number of false alarms was reduced to nearly one-quarter by removing the outliers (3W-DS Validation: 0.68–0.18 h^{-1}) and

TABLE IV
PERFORMANCE OF THE PROPOSED ALGORITHM DURING THE VALIDATION AND TESTING PHASES

Phase	Dataset	Score avg ± STD (%)	SE avg ± std (%)	SP avg ± std (%)	PPV avg ± std (%)	FPRh avg ± std (h^{-1})	aPTime avg ± std (s)	sPTime avg ± std (s)
3W-DS Validation	*Raw data*	$78.8 \pm 3.0^{\dagger}$	84.0 ± 3.4	$86.7 \pm 1.6E{-}14$	77.9 ± 2.2	0.68 ± 0.018	67.9 ± 2.4	34.5 ± 7.3
	Data w/o outliers	$91.8 \pm 2^{\dagger}$	89.0 ± 3.3	96.7 ± 0	94.4 ± 0.82	0.18 ± 0.05	65.4 ± 2.6	40.6 ± 5.1
	Data w/o artifacts	$86.5 \pm 1.9^{\dagger}$	85.3 ± 4.2	93.0 ± 2.5	88.7 ± 4.1	0.16 ± 0.236	70.0 ± 9.4	48.7 ± 10.8
	Data w/o artifacts and outliers	$93.2 \pm 0.06^{\dagger}$	$93.3 \pm 9.1\mathrm{E}{-}15$	$96.7 \pm 1.0\mathrm{E}{-}14$	94.8 ± 0.5	0.15 ± 0.007	61.0 ± 1.0	38.6 ± 5.9
3W-DS Test	*Raw data*	$75.0^{\dagger}$	100	69.2	60.0	0.88	207.1	217.8
	Data w/o outliers	$92.3^{\dagger}$	100	92.3	85.7	0.15	217.6	197.5
	Data w/o artifacts	$83.3^{\dagger}$	83.3	92.3	83.3	0.15	197.1	243.2
	Data w/o artifacts and outliers	$92.3^{\dagger}$	100	92.3	85.7	0.15	243.3	242.5
LOO validation	*Raw data*	$69.6^{\dagger}$	76.2	79.1	64.0	0.75	138.8	147.0
	Data w/o outliers	$93.0^{\dagger}$	95.2	95.4	90.9	0.18	107.9	141.6
	Data w/o artifacts	$87.8^{\dagger}$	85.7	95.4	90.0	0.16	100.9	140.8
	Data w/o artifacts and outliers	$93.0^{\dagger}$	95.2	95.4	90.9	0.14	116.4	155.5

† F-measure (F-m).

to nearly one-fifth by removing both artifacts and outliers (3W-DS Validation: 0.68–0.15 h^{-1}). These results are even more expressive in LOO validation, where a decrease in the FPRh from 0.75 to 0.14 has been observed.

The removal of outliers and artifacts also affected the prediction time of the proposed algorithm. However, while in the 3W-DS validation (aPTime: 67.9–61.0 s) and in the LOO validation (aPTime: 138.8–116.4 s) is observed a decrease in the prediction time, in the 3W-DS test phase, the result was the opposite (aPTime: 207.1 to 243.3 s).

These results show the importance to remove artifacts before parameters are extracted. Additionally, they emphasize the importance of combining the artifacts removal with an outlier removal step, focused on the detection of spurious values provided by the parameter extraction algorithm. Since the post-processing step targets the extracted parameters rather than the characteristics of the analyzed signal, it is capable of detecting unreasonable behaviors caused by the parameter extraction algorithms. Therefore, the combination of both algorithms in the present framework results in a great enhancement of the proposed methods' performance.

2) Prediction Capability: In the 3W-DS validation phase, the proposed algorithm achieved an SE of 93.3%, associated with high specificity (SP: 96.7%) and positive predictive value (PPV: 94.8%). Moreover, the number of false-positives per hour is low (FPRh: 0.15 h^{-1}) and a good prediction time was achieved (aPTime: 61 s). The variance of the achieved prediction times (sPTime) was 38.6 s.

In the LOO validation, the proposed algorithm also achieved high performance (SE: 95.2%; SP: 95.4%; PPV: 90.9%), followed by a low FPRh (0.14 h^{-1}) and a good prediction time (116.4 ± 155.5 s).

In the 3W-DS testing phase, the proposed syncope prediction solution achieved a high SE of 100%, without compromising both specificity (SP: 92.3%) and positive predictive value (PPV: 85.7%). Moreover, the number of false-positives per hour is low (FPRh: 0.15 h^{-1}) and a good prediction time was achieved (aPTime: 243.3 s). The onset of impending syncope was detected in a range of 62 to 629.5 s (presented in Table V) and presented a high variance (sPTime: 242.5 s).

Our results obtained in each validation phase show a minor decrease in the proposed algorithm score, from the 3W-DS validation to the LOO validation phase (93.2% against 93%), and from the 3W-DS validation to 3W-DS test phase (93.2% against 92.3%), as presented in Table IV. However, there was a substantial increase in SE (93.3–100%) and decrease in PPV (94.8–85.7%), from the 3W-DS validation to the 3W-DS test phases. Similarly, there was an increase in SE (93.3–95.2%) and decrease in PPV (94.8–90.9%), from the 3W-DS validation to the LOO validation. The FPRh was similar in both phases ($\approx$0.15 h^{-1}). Contrarily, there was a substantial increase in the prediction time average and standard deviation (65.37 ± 40.6 s to 217 ± 197.45 s), from the 3W-DS validation to the test phase. This discrepancy between the validation and testing performances reflect the differences in the syncope development timings between patients, suggested by the distinct prodomi times presented in Table V.

In order to evaluate the stability of the proposed method, we evaluated its performance in terms of sensitivity and specificity as a function of the adopted threshold. From Fig. 11, it is possible to observe that the optimal threshold identified during the 3W-DS validation phase is within a large range of possible values (from 3.391 to 4.461) yielding the best performance (SE: 100% and SP: 92.3%), presented in Table IV. Moreover, a reduction in Th_0 of at least 0.28 is needed to decrease the specificity below 84% and a rise of at least 1 to set the sensitivity below 70%. These results indicate that the extracted features provide robust discrimination within a large range of optimal thresholds.

TABLE V
PERFORMANCE OF THE PROPOSED ALGORITHM USING THE LOO VALIDATION SCHEME FOR THE 43 PATIENTS

Syncope	PATIENT	TP	FP	TN	FN	Prediction time (s)	Prodomi (s)
No	#05	0	0	1	0	–	–
Yes	#07	1	0	1	0	82	218.1
Yes	#08	1	0	1	0	8	150.1
Yes	#09	1	0	1	0	62.5	98.2
Yes	#10	1	1	0	0	627.5	759.9
No	#11	0	0	1	0	–	–
Yes	#12	1	0	1	0	36	92.7
Yes	#13	1	0	1	0	86	211.4
No	#14	0	0	1	0	–	–
Yes	#15	1	0	1	0	65	92
No	#16	0	1	0	0	–	–
No	#17	0	0	1	0	–	–
Yes	#18	1	0	1	0	24	167
No	#20	0	0	1	0	–	–
No	#21	0	0	1	0	–	–
Yes	#24	1	0	1	0	71	48
No	#25	0	0	1	0	–	–
Yes	#26	1	0	1	0	145	192
No	#27	0	0	1	0	–	–
No	#28	0	0	1	0	–	–
No	#29	0	0	1	0	–	–
No	#30	0	0	1	0	–	–
No	#31	0	0	1	0	–	–
No	#32	0	0	1	0	–	–
Yes	#33	0	0	1	1	–	368
Yes	#34	1	0	1	0	29.5	26
Yes	#36	1	0	1	0	61.5	50
Yes	#37	1	0	1	0	59,5	43
No	#38	0	0	1	0	–	–
Yes	#39	1	0	1	0	66	43
Yes	#40	1	0	1	0	33	195
No	#41	0	0	1	0	–	–
Yes	#42	1	0	1	0	50	53
No	#43	0	0	1	0	–	–
No	#45	0	0	1	0	–	–
Yes	#46	1	0	1	0	155	368
No	#48	0	0	1	0	–	–
No	#49	1	0	1	0	24	30
Yes	#50	1	0	1	0	181	178
Yes	#53	0	0	1	0	–	–
No	#54	0	0	1	0	–	–
No	#55	0	0	1	0	–	–
Yes	#56	1	0	1	0	461.5	495

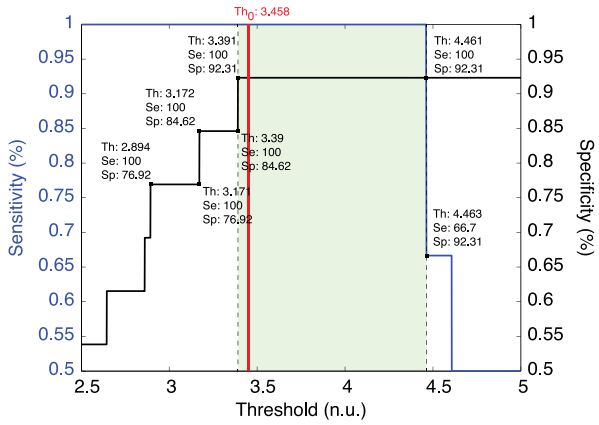

Fig. 11. Representation of the evolution of the sensitivity and specificity performance metrics as a function of the adopted threshold for the 3W-DS test set (data w/o artifacts and outliers)

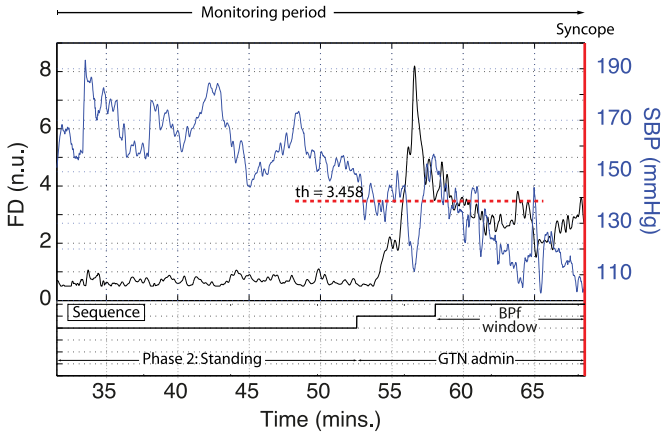

Fig. 12. HUTT of a 17-year-old patient with syncope after GTN administration.

The individual results achieved for each of the 43 patients included in the LOO validation (presented in Table V) show that the proposed solution predicted majority of the syncope events with an acceptable prediction time (over 60 s). This time span is enough to inform the patient for the need to start PCMs or simply to sit/lay down to avoid falling. Moreover, there was a misdetection in patient #10 (FP $= 1$), which led to the decrease in the SP, PPV and increase in FPRh metrics. It is noteworthy to mention that although it was considered as a FP (as a result of an alarm triggered outside the BPf window), this patient suffered a syncope episode subsequently and therefore should not be considered a false-positive. Fig. 12 shows that the optimal threshold is surpassed due to a substantial drop in SBP ($>$40 mmHg) around 57 min, which continues to decrease until the moment of syncope. From Table V, one observes that onset of prodromal symptoms in the majority of the patients preceded syncope detection (range: 3–213 s; 90.2 ± 67.2 s). Yet, prodromal symptoms in the context of the standardized clinical HUTT procedure tend to be more pronounced than during "real-life" onset of syncope. Moreover, in the current study, even the slight symptoms were recorded as prodromal sensations (e.g., mild dizziness or nausea), which in an ambulatory setting might be ignored by the patients.

An important characteristic of our method is the compromise between a high performance, supported by the high values of SE, SP, and PPV (above 85%), and the low false-positive rate per hour, in both validation and testing phases. This is essential in the ambulatory p-health setting, since it helps to avoid mistrust and compromised patient compliance due to false-positive syncope detections. Moreover, the observed prediction times can give patients the ability to act appropriately, e.g., by performing PCMs or simply to sit/lay down avoiding a fall. PCMs act via the increase of sympathetic activity and vascular resistance to raise BP in order to avoid or to delay NMS. According to [44], the effects of PCMs such as the hand grip maneuver were evident after the first 10 s and showed significant BP increases after 2 min. Our results of prediction times ranging from 1 to 9 min might be helpful in an early execution of PCMs and therefore could

TABLE VI
PERFORMANCE OF THE ALGORITHMS PROPOSED IN LITERATURE FOR REAL-TIME SYNCOPE PREDICTION

Dataset	SE avg $\pm$ std (%)	SP avg $\pm$ std (%)	PPV avg $\pm$ std (%)	FPRh avg $\pm$ std (h^{-1})	PTime avg $\pm$ std (s)	Modalities	Number of volunteers
Virag *et al.* [22]	95	93	–	–	128 ± 216	ECG/ABPW	1155
Mereu *et al.* [23]	86.2	89.1	–	–	44.1 ± 6.6	ECG/ABPW	145
Eickolt *et al.* [26]	81	85	–	–	203 ± 227s	ECG/PPG	44
Meyer *et al.* [27]	100	100	100	–	99 ± 108	ECG/PPG	14
Muhlsteff *et al.* [25]	90.48	83.33	82.61	–	77.71 ± 71.78	ECG/PPG	43
Proposed method*	95.2	95.4	90.9	0.14	116.4 ± 155.5	ECG/PPG	43

* LOO validation; data w/o artifacts and outliers.

facilitate the timely administration of effective interventions to prevent or delay NMS.

3) Comparison With the State of the Art: Performing a fair comparison between our method and the other state of the art methods is a challenging task, considering the heterogeneity of the experimental and test protocols, as well as differences in the populations' demographics. However, keeping these topics in our consideration, the comparison and discussion of the methods prediction performance can still be accomplished.

In Table VI, we compare results achieved by our method and methods discussed in literature for real-time prediction of NMS. Visibly, our method outperforms the others in terms of SE, SP, and PPV metrics, excluding the method proposed by Meyer *et al.* [27] (SE/SP/PPV: 100%); however, this study was intended to show basic feasibility under ideal conditions using PAT with a small enrolled number of 14 patients only.

Next to our method is the approach proposed by Virag *et al.* [22], which focused on the analysis of the HR and SBP trends. The results in this study present a similar performance (SE: 95% and SP: 93%). Although no values were provided regarding the PPV and FPRh, the validation of the proposed method on a much larger population (1155 patients) suggests that the presented results are founded on strong statistics, which represents a great advantage compared to the other methods discussed before. Nonetheless, the dependence on the analysis of the arterial blood pressure waveform to assess the SBP trends is still a major disadvantage, since the current available sensors still present limitations regarding their long-term applicability. The remaining algorithms proposed by Mereu *et al.* [23], Eickolt *et al.* [26], and Muehlsteff *et al.* [25] presented similar performances regarding the SE and SP metrics (above 80%).

Considering the prediction time, Eickolt *et al.* [26] reported the best with 203 ± 227 s, followed by Virag *et al.* [22] (128 ± 216 s), and then by our approach (116.4 ± 155.5 s). The lowest prediction time was achieved by Mereu *et al.* [23] with 44.1 ± 6.6 s in advance of a syncope.

E. Wearable Sensors and Real-Life Scenarios

Our NMS prediction algorithm requires the ECG and PPG signals only, which can be easily acquired in real life. For that purpose, within the EU-funded "HeartCycle" project, a wearable monitoring system called "SENSATRON" has been developed. The "SENSATRON" is a multisensor device with a modular design, which can be easily adapted to home and clinical monitoring scenarios. The system can be easily integrated

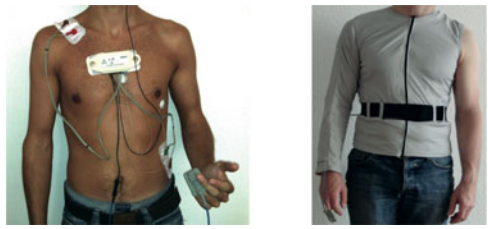

Fig. 13. Left: SENSATRON system attached to a subject by standard adhesive electrodes. Right: functional textile as user-interface developed within HeartCycle for the SENSATRON device.

functional textiles [45], as shown in Fig. 13. Data are stored on an on-board memory card and/or can be wirelessly transmitted via Bluetooth to an external hub.

This device features extended functionalities and acquires an ECG, an impedance cardiogram (ICG), near-infrared PPG, infrared PPG, thoracic inductive plethysmogram, skin temperature as well as sound signals from two thorax locations [46]. Additionally, up to three three-axis acceleration sensors at the thorax, arms or legs provide information on posture and movements. In fact, context information provided by the acceleration sensors will play a fundamental role in the translation of the proposed algorithm in real-life setting, e.g., the detection of motion near the ECG electrodes and PPG sensor. This information can be used in the assistance of the proposed method to improve handling of PPG and ECG motion artifacts and increase the algorithm performance. Additionally, the detection of posture changes provides the temporal windows where orthostatic stabilization is achieved and which time windows shall be used for the normalization of the extracted features. Based on this context information, our algorithm is able to self-calibrate periodically without any human interventions.

V. CONCLUSION AND FUTURE WORK

In this work, a real-time algorithm for syncope prediction based on the evaluation of chronotropic (HR), inotropic (LVET), and vascular tone (SI, RI and PAT) parameters are presented. Features are derived by analysis of ECG and PPG signals only and were combined into a single distance measure. NMS was detected by an appropriately and robust threshold-based approach.

The algorithm was trained and tested on a population of 43 patients using a three-way data split validation scheme. A train/validation subset (30 patients) was used to select the most relevant and least redundant features, the most suitable distance

metric and to define the optimal threshold for syncope prediction. The threshold was found using a fivefold cross-validation approach, repeated 20 times. The prediction capability of the proposed algorithm was evaluated in the test subset of 13 patients (SE: 100%; SP: 92.3%; PPV: 85.7%; FPRh: 0.15 h^{-1}; aPTime: 243.3 s) and in all 43 patients using a leave-one-out cross-validation scheme (SE: 95.2%; SP: 95.4%; PPV: 90.9%; FPRh: 0.14 h^{-1}; aPTime: 116.4 s).

Our results highlight the potential importance of a combined analysis of the extracted parameters in the prediction of impending NMS. Additionally, we demonstrate the robustness of the algorithm approach against artifacts, which will be key feature to transfer our method into to ambulatory and p-health settings.

Future work will focus on the adaptation and deployment of the proposed framework into a continuous monitoring (24/7) wearable system. Moreover, the validation of the algorithm in real-life scenarios such as home care and ambulatory will be also under our concern. Finally, the improvement of the usability of the system and respective sensors will also be one of our primary interests.

ACKNOWLEDGMENT

The authors would like to thank the medical and nursing staff of the Neurocardiology Unit, Division of Cardiology, Pneumology and Angiology, University Düsseldorf, for supporting this study. They would also like to thank especially S. Gläser for excellent technical support.

REFERENCES

[1] A. Moya, R. Sutton, F. Ammirati, J. J. Blanc, M. Brignole, J. B. Dahm, J. C. Deharo, J. Gajek, K. Gjesdal, A. Krahn, M. Massin, M. Pepi, T. Pezawas, R. Ruiz Granell, F. Sarasin, A. Ungar, J. G. van Dijk, E. P. Walma, and W. Wieling, "Guidelines for the diagnosis and management of syncope (version 2009)," *Eur. Heart J.*, vol. 30, pp. 2631–2671, Nov. 2009.

[2] N. Colman, K. Nahm, K. S. Ganzeboom, W. K. Shen, J. Reitsma, M. Linzer, W. Wieling, and H. Kaufmann, "Epidemiology of reflex syncope," *Clin. Auton. Res.*, vol. 14, no. Suppl. 1, pp. 9–17, Oct. 2004.

[3] E. S. Soteriades, J. C. Evans, M. G. Larson, M. H. Chen, L. Chen, E. J. Benjamin, and D. Levy, "Incidence and prognosis of syncope," *New England J. Med.*, vol. 347, pp. 878–885, 2002.

[4] D. M. Lemonick, "Evaluation of syncope in the emergency department," *Amer. J. Clin. Med.*, vol. 7, no. 1, pp. 11–19, 2010.

[5] S. Rosanio, E. R. Schwarz, D. L. Ware, and A. Vitarelli, "Syncope in adults: Systematic review and proposal of a diagnostic and therapeutic algorithm," *Int. J. Cardiol.*, vol. 162, pp. 149–157, 2013.

[6] B. P. Grubb, "Pathophysiology and differential diagnosis of neurocardiogenic syncope," *Amer. J. Cardiol.*, vol. 84, pp. 3–9, 1999.

[7] H. Ouyang and J. Quinn, "Diagnosis and evaluation of syncope in the emergency department," *Emergency Med. Clin. North Amer.*, vol. 28, pp. 471–485, 2010.

[8] N. Lippman, K. M. Stein, and B. B. Lerman, "Failure to decrease parasympathetic tone during upright tilt predicts a positive tilt-table test," *Amer. J. Cardiol.*, vol. 75, pp. 591–595, 1995.

[9] G. Kochiadakis, P. Lees, E. Kanoupakis, N. Igoumenidis, E. Manios, and P. Vardas, "Spectral analysis of heart rate variability in the analysis of autonomic nervous system activity during tilt-table testing in patients with unexplained syncope," in *Proc. Comput. Cardiol.*, 1997, pp. 367–369.

[10] C. A. Morillo, G. J. Klein, D. L. Jones, and R. Yee, "Time and frequency domain analyses of heart rate variability during orthostatic stress in patients with neurally mediated syncope," *Amer. J. Cardiol.*, vol. 74, pp. 1258–1262, 1994.

[11] A. Madrid, C. Moro, E. Marin-Huerta, L. Novo, J. Mestre, J. Lage, and E. Ricoy, "Usefulness of the RR variability in the diagnosis of neurogenic syncope," *Revista Espanola De Cardiol.*, vol. 47, pp. 536–543, 1994.

[12] J. E. Naschitz, I. Rosner, M. Rozenbaum, M. Fields, H. Isseroff, J. P. Babich, E. Zuckerman, N. Elias, D. Yeshurun, S. Naschitz, and E. Sabo, "Patterns of cardiovascular reactivity in disease diagnosis," *QJM*, vol. 97, no. 3, pp. 141–151, Mar. 1, 2004.

[13] Z. Mallat, E. Vicaut, A. Sangaré, J. Verschueren, G. Fontaine, and R. Frank, "Prediction of head-up tilt test result by analysis of early heart rate variations," *Circulation*, vol. 96, pp. 581–584, 1997.

[14] M. Sumiyoshi, Y. Nakata, Y. Mineda, T. Tokano, M. Yasuda, Y. Nakazato, and H. Yamaguchi, "Does an early increase in heart rate during tilting predict the results of passive tilt testing?" *Pacing Clin. Electrophysiol.*, vol. 23, no. 12, pp. 2046–2051, 2000.

[15] C. Kouakam, D. Lacroix, N. Zghal, R. Logier, D. Klug, P. Le Franc, M. Jarwe, and S. Kacet, "Inadequate sympathovagal balance in response to orthostatism in patients with unexplained syncope and a positive head up tilt test," *Heart*, vol. 82, no. 3, pp. 312–318, 1999.

[16] G. A. Ruiz, C. Madoery, F. Arnaldo, C. Menendez, and M. C. Tentori, "Frequency-domain analysis of heart rate variability during positive and negative head-up tilt test: Importance of age," *Pacing Clin. Electrophysiol.*, vol. 23, pp. 325–332, 2000.

[17] K. Efremov, D. Brisinda, A. Venuti, E. Iantorno, C. Cataldi, F. Fioravanti, and R. Fenici, "Heart rate variability analysis during head-up tilt test predicts nitroglycerine-induced syncope," *Open Heart*, vol. 1, no. 1, pp. 1–8, Jun. 1, 2014.

[18] L. Mangin, A. Kobeissi, D. Lelouche, Y. D'Hérouville, P. Mansier, B. Swynghedauw, and I. Macquin-Mavier, "Simultaneous analysis of heart rate variability and myocardial contractility during head-up tilt in patients with vasovagal syncope," *J. Cardiovascular Electrophysiol.*, vol. 12, no. 6, pp. 639–644, 2001.

[19] D. Schang, M. Feuilloy, G. Plantier, J.-O. Fortrat, and P. Nicolas, "Early prediction of unexplained syncope by support vector machines," *Physiol. Meas.*, vol. 28, pp. 185–197, 2007.

[20] E. Bellard, J. O. Fortrat, D. Schang, J. M. Dupuis, J. Victor, and G. Leftheriotis, "Changes in the transthoracic impedance signal predict the outcome of a 70 degrees head-up tilt test," *Clin. Sci.*, vol. 104, pp. 119–126, Feb. 2003.

[21] C. Chun-An, C. Hsin, and C. Hung-Wen, "Early detection of vasovagal syncope in tilt-up test with hemodynamic and autonomic study," in *Proc. Comput. Cardiol.*, 2011, pp. 529–532.

[22] N. Virag, R. Sutton, R. Vetter, T. Markowitz, and M. Erickson, "Prediction of vasovagal syncope from heart rate and blood pressure trend and variability: Experience in 1,155 patients," *Heart Rhythm*, vol. 4, pp. 1375–1382, 2007.

[23] R. Mereu, G. De Barbieri, T. Perrone, A. Mugellini, A. Di Toro, and L. Bernardi, "Heart rate/blood pressure ratio as predictor of neuromediated syncope," *Int. J. Cardiol.*, vol. 167, pp. 1170–1175, 2013.

[24] E. Chung, G. Chen, B. Alexander, and M. Cannesson, "Non-invasive continuous blood pressure monitoring: A review of current applications," *Frontiers Med.*, vol. 7, pp. 91–101, 2013.

[25] J. Muehlsteff, T. Correia, R. Couceiro, P. Carvalho, A. Ritz, C. Eickholt, M. Kelm, and C. Meyer, "Detection of hemodynamic adaptations during impending syncope: Implementation of a robust algorithm based on pulse arrival time measurements only," in *Proc. 35th Annu. Int. Conf. IEEE Eng. Med. Biol. Soc.*, 2013, vol. 2013, pp. 2291–2294.

[26] C. Eickholt, T. Drexel, J. Muehlsteff, A. Ritz, M. Siekiera, K. Kirmanoglou, D.-I. Shin, T. Rassaf, M. Kelm, and C. Meyer, "Neurally mediated syncope prediction based on heart rate and pulse arrival time," *Eur. Heart J.*, vol. 34, no. 1, pp. 161, Aug. 1, 2013.

[27] C. Meyer, G. Morren, J. Muehlsteff, C. Heiss, T. Lauer, P. Schauerte, T. Rassaf, H. Purerfellner, and M. Kelm, "Predicting neurally mediated syncope based on pulse arrival time: Algorithm development and preliminary results," *J. Cardiovascular Electrophysiol.*, vol. 22, no. 9, pp. 1042–1048, 2011.

[28] R. Couceiro, P. Carvalho, R. P. Paiva, J. Muehlsteff, J. Henriques, V. Schulze *et al.*, "Characterization of surrogate parameters for blood pressure regulation in neurally-mediated syncope," in *Proc. 35th Annu. Int. Conf. IEEE Eng. Med. Biol. Soc.*, 2013, pp. 5381–5385.

[29] R. Couceiro, P. Carvalho, R. P. Paiva, J. Henriques, and J. Muehlsteff, "Detection of motion artifact patterns in photoplethysmographic signals based on time and period domain analysis," *Physiol. Meas.*, vol. 35, pp. 2369–2388, 2014.

[30] C.-C. Chang and C.-J. Lin, "LIBSVM: A library for support vector machines," *ACM Trans. Intell. Syst. Technol.*, vol. 2, pp. 27:1–27:27, 2011.

[31] J. Pan and W. J. Tompkins, "A real-time QRS detection algorithm," *IEEE Trans. Biomed. Eng.*, vol. BME-32, no. 3, pp. 230–236, Mar. 1985.

[32] R. Couceiro, P. Carvalho, R. Paiva, J. Henriques, M. Antunes, I. Quintal, and J. Muehlsteff, "Multi-Gaussian fitting for the assessment of left ven-

tricular ejection time from the Photoplethysmogram," in *Proc. 34th Annu. Int. Conf. IEEE Eng. Med. Biol. Soc.*, San Diego, 2012, pp. 3951–3954.
[33] Y. Sun, K. Chan, and S. Krishnan, "Characteristic wave detection in ECG signal using morphological transform," *BMC Cardiovascular Disorders*, vol. 5, no. 28, pp. 1–7, 2005.
[34] U. Rubins, "Finger and ear photoplethysmogram waveform analysis by fitting with Gaussians," *Med. Biol. Eng. Comput.*, vol. 46, pp. 1271–1276, 2008.
[35] M. Baruch, D. Warburton, S. Bredin, A. Cote, D. Gerdt, and C. Adkins, "Pulse decomposition analysis of the digital arterial pulse during hemorrhage simulation," *Nonlinear Biomed. Phys.*, vol. 5, no. 1, pp. 1–15, 2011.
[36] R. A. Waltz, J. L. Morales, J. Nocedal, and D. Orban, "An interior algorithm for nonlinear optimization that combines line search and trust region steps," *Math. Program.*, vol. 107, pp. 391–408, 2006.
[37] J. Muehlsteff, A. Ritz, T. Drexel, C. Eickholt, P. Carvalho, R. Couceiro, M. Kelm, and C. Meyer, "Pulse arrival time as surrogate for systolic blood pressure changes during impending neurally mediated syncope," in *Proc. 34th Annu. Int. Conf. IEEE Eng. Med. Biol. Soc.*, 2012, pp. 4283–4286.
[38] C. Meyer, G. Morren, J. Muehlsteff, C. Heiss, T. Lauer, P. Schauerte, T. Rassaf, H. Purerfellner, and M. Kelm, "Predicting neurally mediated syncope based on pulse arrival time: Algorithm development and preliminary results," *J. Cardiovascular Electrophysiol.*, vol. 22, pp. 1042–1048, Sep. 2011.
[39] S. S. DeLoach and R. R. Townsend, "Vascular stiffness: Its measurement and significance for epidemiologic and outcome studies," *Clin. J. Amer. Soc. Nephrol.*, vol. 3, pp. 184–192, 2008.
[40] O. Salem, L. Yaning, and A. Mehaoua, "A lightweight anomaly detection framework for medical wireless sensor networks," in *Proc. IEEE Wireless Commun. Netw. Conf.*, 2013, pp. 4358–4363.
[41] R. Wang and K. Tang, "Feature selection for maximizing the area under the ROC curve," in *Proc. IEEE Int. Conf. Data Mining Workshops*, 2009, pp. 400–405.
[42] *Philips MP50*. (2008). [Online]. Available: www.philips.com
[43] *Taskforce monitor*. (2008). [Online]. Available: www.cnssystems.com
[44] M. Brignole, F. Croci, C. Menozzi, A. Solano, P. Donateo, D. Oddone, E. Puggioni, and G. Lolli, "Isometric arm counter-pressure maneuvers to abort impending vasovagal syncope," *J. Amer. Coll. Cardiol.*, vol. 40, no. 11, pp. 2053–2059, 2002.
[45] H. Reiter, J. Muehlsteff, and A. Sipila, "Medical application and clinical validation for reliable and trustworthy physiological monitoring using functional textiles: Experience from the HeartCycle and MyHeart project," in *Proc. 33th Annu. Int. Conf. IEEE Eng. Med. Biol. Soc.*, 2011, pp. 3270–3273.
[46] J. Muehlsteff, P. Carvalho, J. Henriques, R. P. Paiva, and H. Reiter, "Cardiac status assessment with a multi-signal device for improved home-based congestive heart failure management," in *Proc. 33th Annu. Int. Conf. IEEE Eng. Med. Biol. Soc.*, 2011, pp. 876–879.

Authors' photographs and biographies not available at the time of publication.